Visual servoing frameworks for microassembly of hybrid MEMS

Stephen J. Ralis

Department of Mechanical Engineering
University of Illinois at Chicago
Chicago, Illinois 60607 USA

Barmeshwar Vikramaditya Bradley J. Nelson

Department of Mechanical Engineering
University of Minnesota
Minneapolis, Minnesota 55455 USA

ABSTRACT

In this paper we present a novel visual servoing framework for assembly of hybrid microelectromechanical systems (MEMS). The framework incorporates a supervisory logic-based controller that allows the use of multiple visual sensors in order to execute an assembly task. The introduction of multiple visual sensor arrays allows motion of microassembly tasks to initially be controlled "globally" and then locally using a "high precision" view. We use the technique of depth-from-focus to visually servo along the optical axis. This gives us the ability to perform full 3D micropositioning under visual control. The supervisory logic-based controller selects the relevant sensor to be used at a particular stage in the assembly process, which allows us to take full advantage of the individual sensor's attributes such as field-of-view and resolution. The combination of robust visual tracking and depth estimation within a supervisory control architecture is used to perform high-speed, automatic microinsertions. We present results for the micro insertion task performed under this framework to demonstrate it's feasibility in assembly of MEMS.

Keywords: Depth-from-focus, MEMS, Microassembly, Sensor integration, Supervisory logic-based control, Visual servoing.

1. INTRODUCTION

As MEMS devices become more functional and more complex, the need for assembling hybrid MEMS devices, such as miniature drug pumps, actuators,[20,24] sensors,[21,25] optical devices,[3] etc. becomes apparent. Packaging these devices in order to protect them from their operating environment while allowing for interfaces to the necessary electrical, mechanical, and fluidic elements is also important. The eventual commercial success of hybrid MEMS technology, as well as other technologies dealing in microscales, requires that the handling of these microparts be performed automatically in order to preserve potential economic benefits.

In a macro domain, visually servoed assembly[11,22] has been shown to effectively compensate for uncertainty in the calibration of camera-lens systems, manipulators, and workspaces. However, in a micro domain precise calibration is highly dependent on precisely modeled kinematics which are subject to thermal growth errors. Two common techniques for compensating for thermal errors include either the use of expensive cooling systems, or waiting hours for the thermal equilibrium of the device to stabilize. Slocum[16] points out that "thermal growth errors are typically the most difficult to control and compensate". Because these types of factors greatly affect the cost and reliability of precision assembly machines, real-time visual

B.J.N. (correspondence): Email: nelson@me.umn.edu; Telephone: 612-625-0077; Fax: 612-624-1398
Other author information: Stephen J. Ralis (sralis1@uic.edu), Barmeshwar Vikramaditya (bvikra1@uic.edu).

feedback can be used effectively and economically as a component of a microassembly system. In addition to thermal growth, it can also compensate for the incomplete understanding of the physics of the micro domain.

In this paper, we present a supervisory logic-based control architecture that integrates multiple visual sensors. The architecture allows for switching sensing modes based on the task to be performed for optimal speed and repeatability. Experimental results demonstrate the feasibility of this architecture in performing automated micro insertion under visual control.

2. MICROASSEMBLY

2.1. The Mechanics of Microassembly

Microassembly tasks differ from their macro counterparts because of the vastly different physics in the micro domain which has not been completely characterized. This introduces the requirement for sensor based manipulation techniques. The mechanics of manipulation in the macro world are predictable and can be modeled accurately. For example, when a gripper opens, forces due to gravity cause the part to drop. This predictability has enabled the success of many complex sensorless manipulation strategies. In the micro world, forces other than gravity may dominate. For example, a possible microassembly scenario is one in which electrostatic forces dominate and cause a part to "jump" into a gripper before contact actually occurs. As the gripper opens to place the micropart at its goal, the part may stick to the gripper fingers and not remain at the desired location.[2] If humidity in the room happens to be high, surface tension effects can dominate gravitational forces, and the part would also remain stuck to the gripper.[1] It is estimated that for parts with major dimensions below 100μm, gravity is negligible and, electrostatic forces, Van der Waals forces, and surface tension dominate.[1] However, this is only a rough estimate and depends on several factors, such as mass density, surface roughness, humidity, part geometry, electrical grounding, etc. Although particular forces can be defined, their effect on the process can only be roughly estimated. This makes the task of microassembly quite difficult.

2.2. Related Work in Microassembly

Currently, microdevices requiring complex manipulation are assembled by hand using an optical microscopes and probes or small tweezers, and is essentially a form of teleoperated micromanipulation. In the Microfabrication Applications Laboratory, we have assembled many different microdevices by hand using optical microscopes. Some of the devices include miniature fiber optic assemblies, micropumps, and electron columns for miniature scanning electron microscopes.[3] We seek to develop robust manipulation strategies for automating these types of assembly tasks.

Many researchers are actively pursuing strategies for manipulating micron sized objects for various applications. For example, researchers have used feedback from a scanning electron microscope (SEM) to teleoperatively guide micromanipulation;[15] systems have been developed for accurate positioning of optical elements;[26] techniques for remote teleoperation of micro/milli sized structures have been developed;[5] vision based methods have been proposed;[6,17,19] and microassembly workcells are being built,[8] to name a few of the efforts in this area.

3. SYSTEM MODELING AND CONTROL

3.1. Camera Model

In formulating the visual servoing component of our system, we map the task space coordinates into the sensor space through a Jacobian mapping. We desire a Jacobian for the camera-lens system of the form

$$\dot{\boldsymbol{x}}_S = \boldsymbol{J}_v(\phi)\dot{\boldsymbol{X}}_T \tag{1}$$

where $\dot{\boldsymbol{x}}_S$ is a velocity vector in sensor space; $\boldsymbol{J}_v(\phi)$ is the image Jacobian matrix and is a function of the extrinsic and intrinsic parameters of the vision sensor as well as the number of features tracked and their locations on the image plane; and $\dot{\boldsymbol{X}}_T$ is a velocity vector in task space. For an eye-in-hand camera, mounted on a microscope, that is allowed to translate and rotate,

$\boldsymbol{J}_v(\phi)$ is of the form

$$\boldsymbol{J}_v = \begin{bmatrix} \frac{f}{s_x Z_c} & 0 & \frac{-x_s}{Z_c} & \frac{-Y_T x_s}{Z_c} & \left[\frac{fZ_T}{s_x Z_c} + \frac{X_T x_s}{Z_c}\right] & \frac{-fY_T}{s_x Z_c} \\ 0 & \frac{f}{s_y Z_c} & \frac{-y_s}{Z_c} & \left[\frac{fZ_T}{s_y Z_c} + \frac{Y_T y_s}{Z_c}\right] & \frac{X_T y_s}{Z_c} & \frac{fX_T}{s_Y Z_c} \end{bmatrix} \tag{2}$$

where s_x and s_y are pixel dimension on the CCD; x_s and y_s are the actual image coordinates of a feature; (X_C,Y_C,Z_C) is the image vector with respect to the camera; (X_T,Y_T,Z_T) is the image vector with respect to the task space; and f is the focal length.

Generally several features are tracked. Thus, for n feature points the Jacobian is of the form

$$\boldsymbol{J}_v = \left[J_1(t) \; .... \; J_n(t)\right]^T \tag{3}$$

where $J_i(t)$ is the Jacobian matrix for each feature given by (2). A complete derivation of (2) can be found in our previously published work.[19]

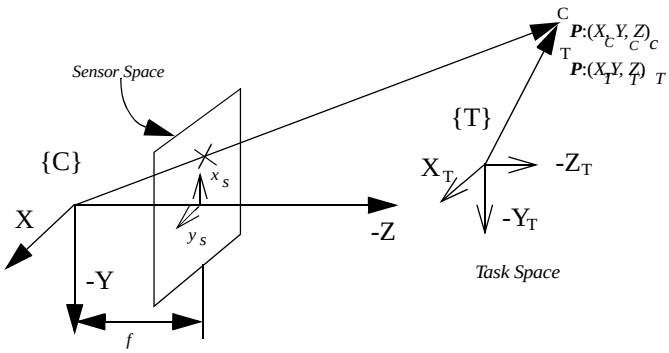

Figure 1. Camera and Task space coordinate reference.

3.2. Optimal Controller

The state equation for the visual servoing system is created by discretizing (1) and rewriting the discretized equation as

$$\boldsymbol{x}(k+1) = \boldsymbol{x}(k) + T\boldsymbol{J}_v(k)\boldsymbol{u}(k) \tag{4}$$

where $\boldsymbol{x}(k) \in R^{2M}$ (M is the number of features being tracked); T is the sampling period of the vision system; and $\boldsymbol{u}(k) = \left[\dot{X}_T \; \dot{Y}_T \; \dot{Z}_T \; \omega_{X_T} \; \omega_{Y_T} \; \omega_{Z_T}\right]^T$ is a velocity in task manipulator end-effector velocity. The Jacobian is written as $\boldsymbol{J}_v(k)$ in order to emphasize its time varying nature due to the changing feature coordinates on the image plane. The intrinsic parameters of the camera-lens system are constant for the experimental results to be presented.

The control objective of the system is to control end-effector motion in order to place the image plane coordinates of features on the target at some desired position. The desired image plane coordinates could be constant or changing with time. The control strategy used to achieve the control objective is based on the minimization of an objective function that places a cost on errors in feature positions, $[\boldsymbol{x}(k+1) - \boldsymbol{x}_D(k+1)]$, and a cost on providing control energy or input, $\boldsymbol{u}(k)$.

$$F(k+1) = [\boldsymbol{x}(k+1) - \boldsymbol{x}_D(k+1)]^T \boldsymbol{Q}[\boldsymbol{x}(k+1) - \boldsymbol{x}_D(k+1)] + \boldsymbol{u}^T(k)\boldsymbol{L}\boldsymbol{u}(k) \tag{5}$$

This expression is minimized with respect to the current control input $\boldsymbol{u}(k)$. The end result yields the following expression for the control input.

$$\boldsymbol{u}(k) = -\left(T\boldsymbol{J}_v{}^T(k)\boldsymbol{Q}T\boldsymbol{J}_v(k) + \boldsymbol{L}\right)^{-1} T\boldsymbol{J}_v{}^T(k)\boldsymbol{Q}[\boldsymbol{x}(k) - \boldsymbol{x}_D(k+1)] \tag{6}$$

The weighting matrices $\boldsymbol{Q}$ and $\boldsymbol{L}$ allow the user to place more or less emphasis on the feature error and the control input. Extensions to this system model and control derivations that account for system delays, modeling and control inaccuracies, and measurement noise have been experimentally investigated.[12]

3.3. Supervisory Logic-based Controller

Sensory feedback from multiple sensors provides rich information about the task space. We use multiple vision sensors that have different operating regimes in terms of resolution and field-of-view. We switch the sensory information based on a logic-based supervisory controller.[23] The appropriate sensor is determined by the controller and the control system parameters are configured for the active sensor. The architecture is depicted in Figure 2.

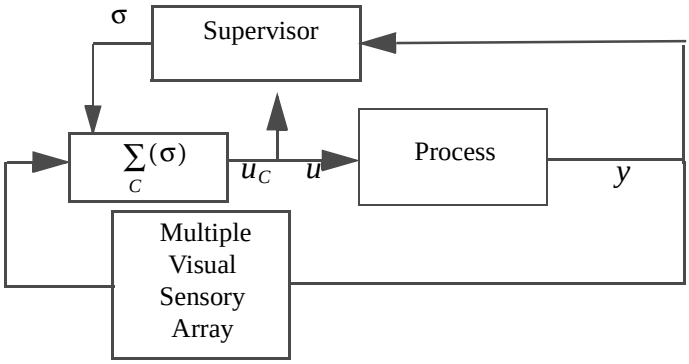

Figure 2. Supervisory logic-based control architecture.

Realizing that at every instant in time, only one control input is required, a single controller with adjustable parameters can be formulated in state-space form as

$$\begin{aligned} \dot{\boldsymbol{x}}_S &= A_\sigma \boldsymbol{x}_S + \boldsymbol{J}_v \boldsymbol{u} \\ \boldsymbol{u}_C &= F_\sigma \boldsymbol{x}_S \end{aligned} \tag{7}$$

where $\dot{\boldsymbol{x}}_S$ is sensor space velocity; $\boldsymbol{x}_S$ is the sensor space position; and $\boldsymbol{u}_C$ is the input task space velocities (see Section 3.2.) The supervisory signal, σ, is transmitted to the controller, $\sum_c(\sigma)$, that selects the controller input to the system based on the visual sensory feedback. The matrice A is $\boldsymbol{I}_2$; $\boldsymbol{J}_v$ is the image Jacobian; but the input $\boldsymbol{u}_C$ changes with respect to the signal output of the supervisor that switches the control gains, F_σ. This provides real time logic-based switching of multiple controllers via feedback of the process from multiple sensors.

4. IMAGE PROCESSING

4.1. Feature Tracking on the Image Plane

The measurement of the motion of the features on the image plane must be done continuously and quickly. The method used to measure this motion is based on an optical flow technique called Sum-of-Squared Differences (SSD). The inherent assumption is that the intensities around a feature remain constant as that feature moves across the image plane. The displacement of a point $p_a = (x_S, y_S)$ at the next time increment to $p_a = (x_S + \Delta x, y_S + \Delta y)$, is determined by finding the displacement Δx=(Δx,Δy) which minimizes the SSD measure e(p_a, Δx). A pyramidal search scheme is used to reduce the search space. A more complete description of the algorithm and its implementation can be found in.[11]

4.2. Servoing Along the Optical Axis

4.2.1. Depth-of-Field

Micro assembly tasks require highly magnified views of the task space to provide submicron accuracy. High magnification optical systems usually have a high numerical aperture and thus have a very small depth-of-field. Figure 3 shows the insertion probe when it is in focus and when it is out of focus, the depth-of-field being approximately 90μm. This limited depth-of-filed can be exploited to measure depth from the camera using techniques of depth-from-focus/defocus.

Depth-from-focus has been studied extensively as a technique for recovering depth estimates from the limited depth-of-field exhibited by optical lenses.[4,10,13] The depth of field formulation for a pinhole camera system is given as

Figure 3. Images of the defocused and focused probe.

$$\Delta = Daf\left(\frac{1}{af - p(D-f)} - \frac{1}{af + p(D-f)}\right) \tag{8}$$

where Δ is the depth-of-field, D is the focus distance, a is the lens aperture, f is the lens focal length, and p is the minimum of the x and y pixel dimensions on the CCD array.[18]

The above formulation is valid for optical systems approximated by a pinhole camera model. However, for high numerical aperture systems the wave nature of light comes into play and diffractive effects result in a depth-of-field formulation given as

$$\Delta = \frac{\lambda_0 n}{2A^2} + \frac{n}{7mA} \tag{9}$$

where λ_0 is the wavelength of light in a vacuum, n is the diffractive index of the lenses, A is the numerical aperture of the lens system, and m is the magnification of the optical system.[7] The significance of this equation is that the depth-of-field is on the order of the wavelength of light. This provides the ability to calculate depth of objects in the micro domain with accuracy approaching of the order of wavelength of light.

4.2.2. Focus Measure

Generally focused images are characterized by high spatial frequency content, while blurred images have attenuated high frequency content. If we consider the histogram corresponding to the focused and defocused probe shown in Figure 3, we see a response as shown in Figure 4. The histogram corresponding to the focused probe has intensity variations from 100 to 215 approximately. Two notable peaks illustrate the focused characteristic of the feature (left peak) as well as the background (right peak). As a result, we can use a histogram to characterize the level of focus for the feature of interest. A histogram of the region of interest is continuously monitored, which allows us to servo along the optical axis before a final insertion operation is carried out.

The pixels around the edge of the focused feature produce the dip between the peaks. A threshold gray level value may be chosen in the trough region that will characterize a reasonable boundary for the focused object from the background.[9,14]

5. EXPERIMENTAL RESULTS

5.1. Hardware Setup

Experiments were conducted with the micro insertion workstation shown in Figure 5. The workstation is centered around a Daedal positioning platform with independent X, Y, and Z motion powered by Yaskawa E-series servodrives and servomotors. The multiple visual sensory array consists of a Marshall Electronics V-X0071 video camera on a chip and a Sony XC-75 CCD camera using a microscope zoom lens (Marshall Electronics Inc. V48612MZ). Image processing and visual servoing

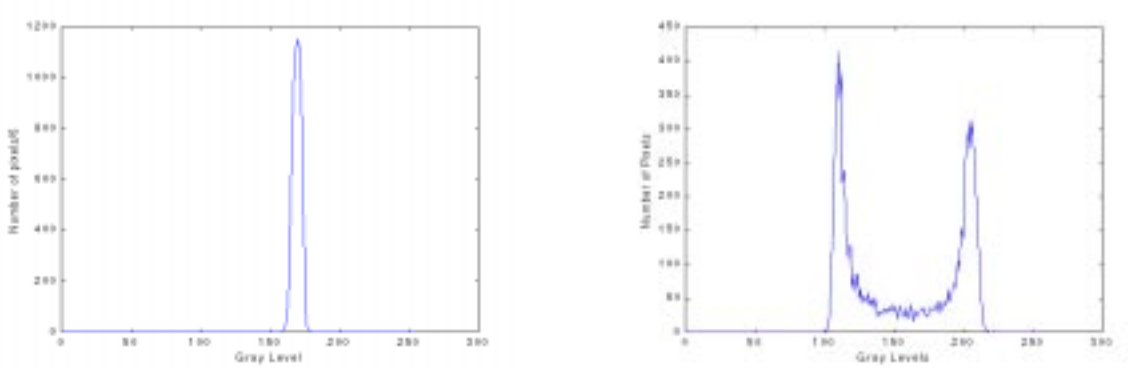

Figure 4. Histogram of defocused region and focused region corresponding to Figure 3.

control calculations were performed with a vision system consisting of a digitizer and framegrabber based on Texas Instruments TMS320C40 DSP's, supplied by Traquair Data Systems. The vision system is able to track up to 5 16x16 feature templates at 30Hz. Motion control was accomplished utilizing a programmable multi-axis controller (PMAC-PC) servo motion card manufactured by Delta Tau.

Table I: Calibration Data

	Global Visual Sensor			Narrow Visual Sensor		
	Pixels	Encoder Counts	Actual Displacement	Pixels	Encoder Counts	Actual displacement
X	1	34.68	17.84	1	4.30	2.21
Y	1	52.06	26.78			

5.2. Visual Servoing Results

The micropositioning of the system was categorized into three visual servoing steps: low precision visual servoing, utilizing the global view for feedback; high precision depth servoing using the histogram information to visually servo along the optical axis; and the final high precision visual servoing in the XY task space with a blind insertion.

Repetitive micropositioning of a probe to numerous holes on a machined template was accomplished. Resolution of the multiple visual sensory array is listed in Table I. The holes are machined to 254μm in diameter and are separated by 1mm. in both the X and Y directions. The probe is tapered to 228.6μm in diameter.

Optimal performance was achieved by tuning the values of the diagonal terms in the control gain matrix $\boldsymbol{Q}$ in (6) for each of the three visually servoed steps. Adjustments in $\boldsymbol{Q}$ between magnification were required in order to achieve optimal performance. The supervisory logic-based controller selects the control input based on the output of the system enabling coarse-to-fine pre-tuned visual servoing.

Low precision visual servoing, depicted in Figure 6, was accomplished in 0.36s with a precision of 17.9μm in X and 26.8μm. Precision servoing along the optical axis was completed in 0.25s. In Figure 7 the initial and final histograms are shown that correspond to the defocused and focused image of the probe. The final high precision visual servoing was completed in 0.25s with a precision of 2.21μm in X and Y. The initial and final states are illustrated in Figure 8.

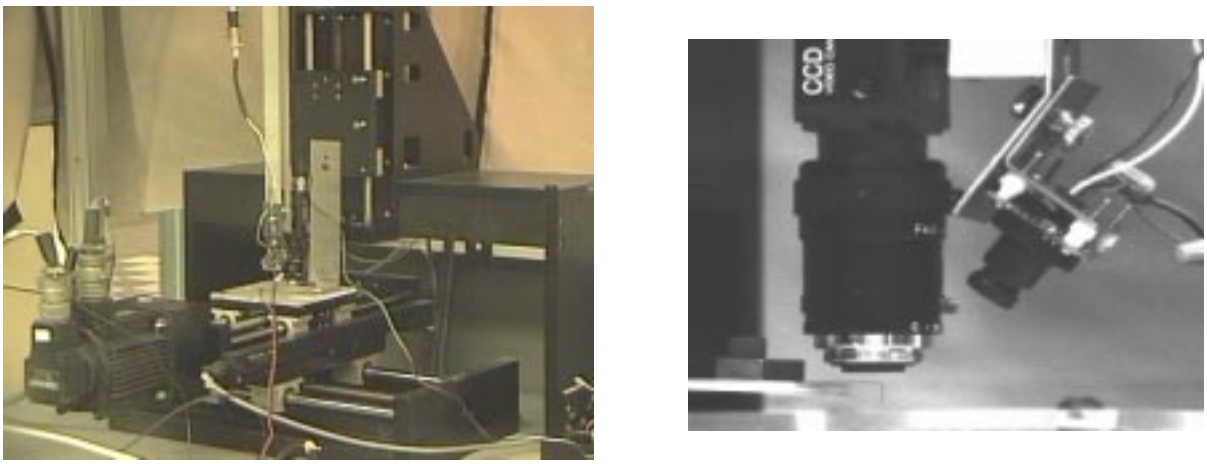

Figure 5. Micro insertion workstation and close-up view of the multiple visual sensors.

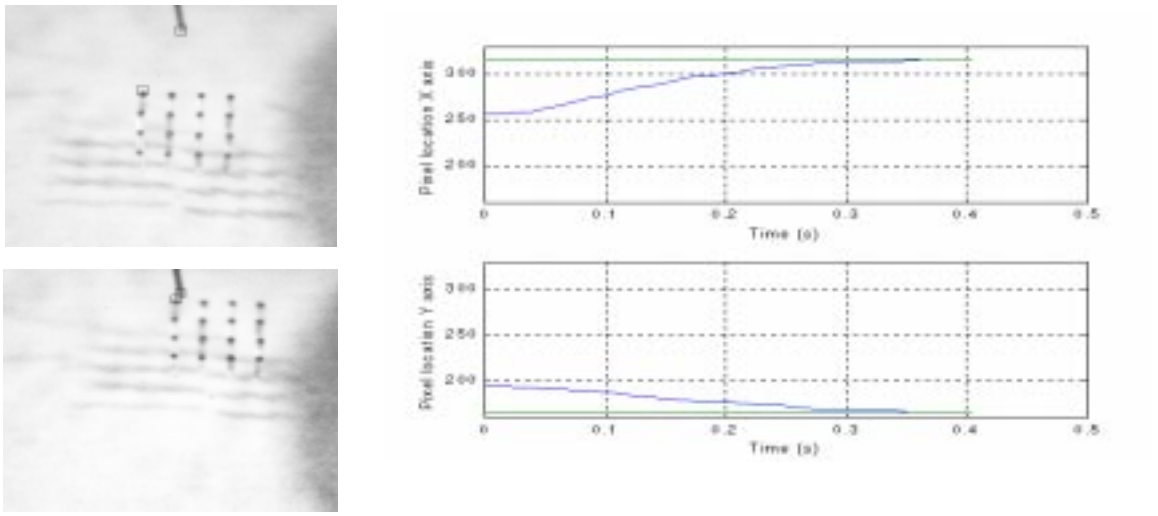

Figure 6. Low precision visual servoing: Top left - before visual servoing; Bottom left - after visual servoing; Right - acquisition of desired probe location by visual servoing of X & Y axes.

5.3. Quantitative Positional Results

This section addresses characteristics of the complete motion profile. Figure 9 portrays the complete range of motion for all three axis of insertion of the probe into the closest hole. This includes low precision visual servoing in X and Y, servoing along Z-axis using depth-from-focus and, finally, high precision visual servoing in X and Y. The total time for one insertion is approximately 0.9s. This procedure demonstrates real time visual servoing using a logic-based switching control strategy. Each region depicted in Figure 9 is representative of one of the visual servoing strategies: (1) low precision visual servoing; (2) servoing in depth using histogram information; (3) high precision visual servoing. The X and Y axes move approximately

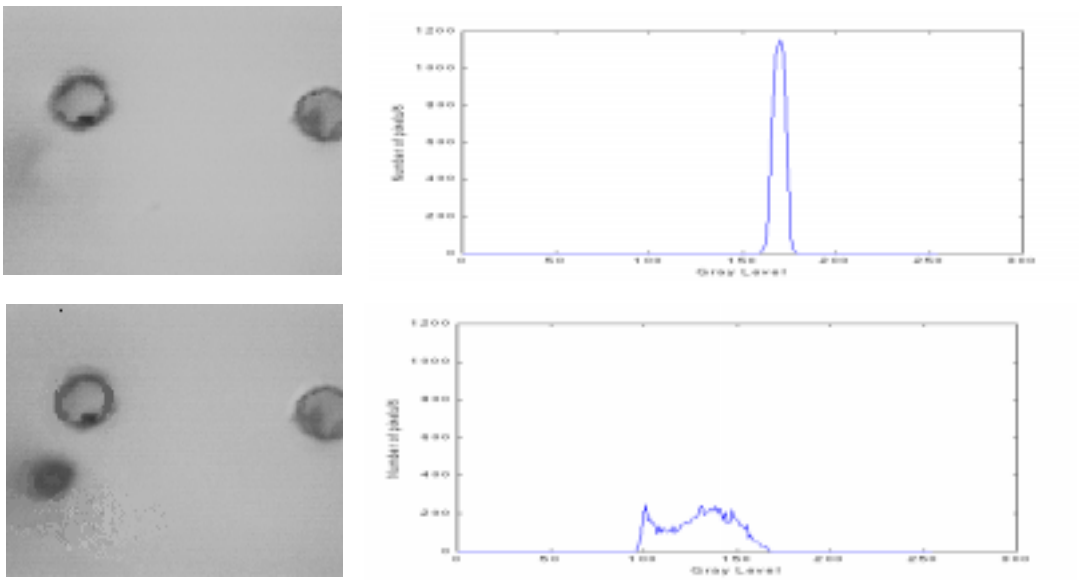

Figure 7. Image intensity Z-axis visually servoed motion: Top left - before visual servoing; Bottom left - after visual servoing; Top right - histogram of defocused state: Bottom right - Histogram of focused state.

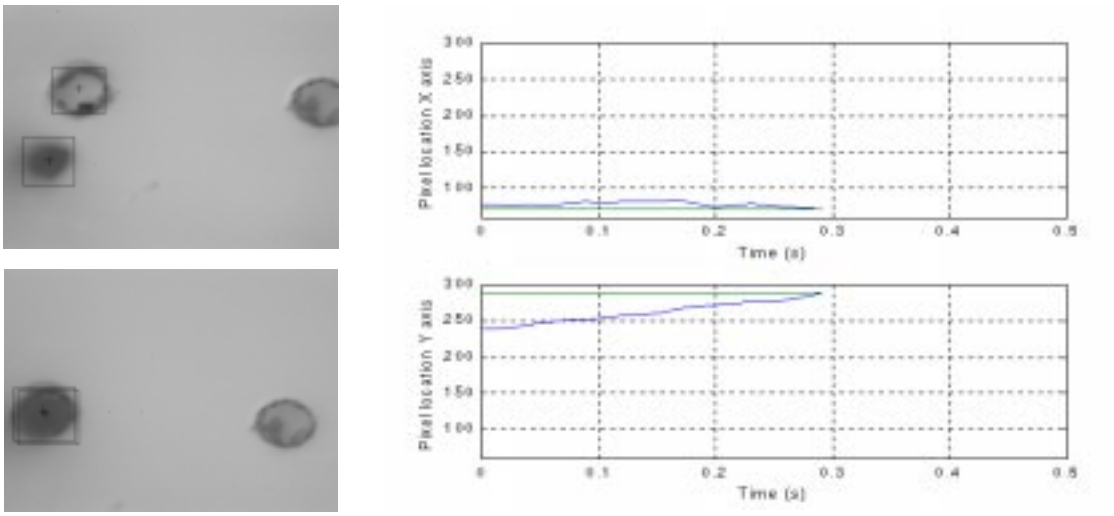

Figure 8. High precision visual servoing: Top left - before visual servoing; Bottom left - after visual servoing; Right - acquisition of desired probe location by visual servoing of X & Y axes.

670µ*m* in 0.36*s* (1.86*mm/s*) to the desired probe location in the low precision view. The Z-axis then positions the probe by 230µ*m* into focus in 0.25*s* (0.92*mm/s*) and finally, the high precision servoing task servoes the X axis 20µ*m* and the Y-axis 130µ*m* in 0.29*s* (0.448*mm/s*). Figure 9 displays an additional motion of Z-axis motion at the end of the insertion procedure. This is the blind insertion carried out after the precision XY servo stage. Once insertion is complete, the system resets itself and begins insertion into the next predetermined target hole.

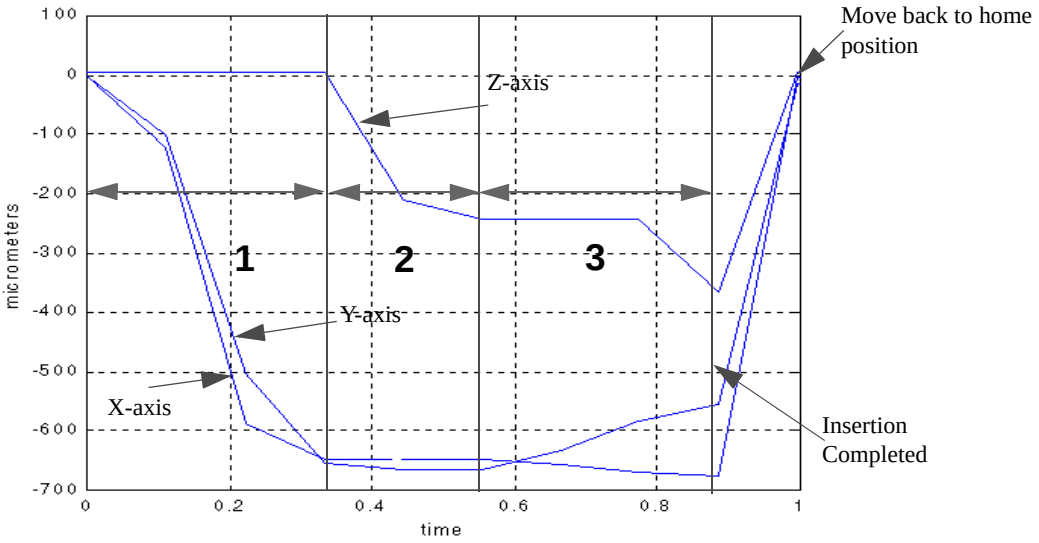

Figure 9. Complete range of motion of one insertion

6. CONCLUSION

The integration of multiple sensory array and a supervisory logic-based controller shows promise in overcoming a technology barrier to the manipulation of micron-sized objects, and to the automated microassembly of hybrid MEMS devices in particular. In this paper, we have theoretically and experimentally investigated the use of image-based visual servoing using optical flow and image intensity information to robustly control motion down to micron repeatability. This highly precise repeatability was achieved with visually servoed motion at relatively high speeds between 0.448 - 1.90 mm/s over a large range of motion of 4x4x4cm^3. The integration framework can be used within an automated or a supervisory system. The goal of this work is to develop robotic micromanipulation strategies that compensate for modeling uncertainties inherent in the micro-domain, such as thermal growth, humidity effects, electrostatic forces, etc.

ACKNOWLEDGEMENTS

This research was supported in part by the National Science Foundation through Grant Numbers IRI-9612329, CDA-9616757, and IRI-9702777, by the Office of Naval Research through Grant Number N00014-97-1-0668, and by DARPA through Grant Number N66001-97-1-8911.

REFERENCES

[1] F. Arai, D. Ando, T. Fukuda, “Micro Manipulation Based on Micro Physics-Strategy Based on Attractive Force Reduction and Stress Measurement,” *Proc. 1995 IEEE/RSJ Int. Conf. on Intelligent Robots and Sys. (IROS95)*, 2:236-241, Pittsburgh, August 5-9, 1995.
[2] R.S. Fearing, “Survey of Sticking Effects for Micro Parts Handling,” *Proc. 1995 IEEE/RSJ Int. Conf. on Intelligent Robots and Sys. (IROS95)*, 2:212-217, Pittsburgh, August 5-9, 1995.
[3] A. D. Feinerman, D. A. Crewe, D. C. Perng, S. E. Shoaf, A. V. Crewe, “Sub-centimeter micromachined electron microscope”, *Journal of Vacuum Science and Technology*, A, 10(4), pp. 611-616, 1992.
[4] P. Grossman P., “Depth from focus”, *Pattern Recognition Letters*, 5:63-69, 1987.
[5] B. Hannaford, J. Hewitt, T. Maneewarn, S. Venema, M. Appleby, and R. Ehsresman, “Telerobotic remote handling of protein crystals,” *Proc. 1997 IEEE Int. Conf. on Robotics and Automation*, 1010-1015, 1997.
[6] K. Koyano and T. Sato, “Micro object handling system with concentrated visual fields and new handling skills,” *Proc. 1996 IEEE INt. Conf. on Robotics and Automation*, pp. 2541-2548, 1996.
[7] L.C. Martin, *The Theory of the Microscope*, American Elsevier, 1966.

[8] A. Menciassi, M.C. Carroza, C. Ristori, G. Tiezzi, and P. Dario, “A workstation for manipulation of micron sized objects,” *Proc. 1997 8th Int. Conf. on Advanced Robotics*, pp. 253-258, 1997.
[9] M. Mendelsohn, B. Mayatt, J. Prewitt, R. Bostrom, R. Holcomb, “Digital Transformation and Computer Analysis of Microscope”, *Advances in Optical and Electron Microscopy*, V2, Academic Press, London, 1968.
[10] Y. Nakagawa, H.K. Nayar, “Shape from focus: An effective approach for rough surfaces”, *Proc. IEEE Conf. on Robotics and Automation*, p.218-225, 1990.
[11] B. Nelson, N.P. Papanikolopoulos, and P.K. Khosla, “Visual servoing for robotic assembly,” *Visual Servoing—Real-Time Control of Robot Manipulators Based on Visual Sensory Feedback*. ed. K. Hashimoto. River Edge, NJ:World Scientific Publishing Co. Pte. Ltd. pp. 139-164, 1993.
[12] N.P. Papanikolopoulos, Nelson, B. and Khosla, P.K., “Full 3-d tracking using the controlled active vision paradigm,” *Proc. 1992 IEEE Int. Symp. on Intelligent Control (ISIC-92)*, pp. 267-274, 1992.
[13] A.P. Pentland, “A new sense for depth of field”, *IEEE Trans. PAMI*, 9(4):523-531, 1987.
[14] J. Prewiit, M. Mendelsohn, “The Analysis of Cell Images”, *Annals of the New York Academy of Sciences*, 128:1035-1053, Jan. 1966.
[15] T. Sato, T. Kameya, H. Miyazaki, Y. Hatamura, “Hand-eye System in the Nano Manipulation World,” *Proc. 1995 IEEE Int. Conf. on Robotics and Automation*, pp. 59-66, 1995.
[16] A.H. Slocum, *Precision Machine Design*, Prentice Hall, 1992.
[17] A. Sulzmann, J.M. Breguet, J. Jacot, “Micromotor assembly using high accurate optical vision feedback for microrobot relative 3D displacement in submicron range,” *Proc. 1997 Int. Conf. on Solid-State Sensors and Actuators (Transducers 97)*, 279-282, 1997.
[18] K. Tarabanis., R,Y, Tsai, P.K. Allen, “Satisfying the Resolution Constraint in the “MVP” Machine Vision Planning System”, *Proc of the 1990 DARPA Image Understanding Workshop*, p.850-860, 1990.
[19] B. Vikramaditya and B.J. Nelson, “Visually Guided Microassembly Using Optical Microscopes and Active Vision Techniques,” *Proc. 1997 IEEE Int. Conf. on Robotics and Automation*, pp. 3172-3177, Albuquerque, April 21-27, 1997.
[20] K. I. Arai, T. Honda, “Micromagnetic actuators”, *Robotica*, 14:477-481, Sept. 1996.
[21] T. M. Betzner, J. R. Doty, A. M. A. Hamad, H. T. Henderson, F. G. Berger, “Structural design and characteristics of a thermally isolated sensitivity enhanced bulk micromachined silicon flow sensor”, *Journal of Micromechanics and Microengineering*, 6(2):217-227, 1996.
[22] J. T. Feddemma, C. S. G. Lee, O. R. Mitchell, “Weighted selection of image features for resolved rate visual feedback control”, *IEEE Trans. on Robotics and Automation*, 1(1):31-47, 1991.
[23] M. Fu, B. R. Barmish, “Adaptive stabilization of linear systems via switching controls”, *IEEE Trans. on Automatic Control*; p.1097-1103, Dec. 1986.
[24] H. Fujita, “Micro Actuators for Micro-Motion Systems”, *Integrated Micro-Motion Systems- Micromachining, Control and Applications*, Ed. F. Harashima, p.279-296, Elsevier Science Publishers, 1990.
[25] D. Haronian, N. C. MacDonald, “A microelectromechanics-based frequency-signature sensor”, *Sensor and Actuators*, A, 53:288-298, 1996.
[26] Y.Yamagata and T. Higuchi, “A Micropositioning Device for Precision Automatic Assembly using Impact”, *IEEE Int. Conf. on Robotics and Automation*, pp. 610-615, 1995.